# ARTICLES

## Neutron phase echo

R. Clothier,* H. Kaiser, and S. A. Werner
*Physics Department and Research Reactor Facility, University of Missouri–Columbia, Columbia, Missouri 65211*

H. Rauch and H. Wölwitsch
*Atominstitut der Österreichischen Universitäten, A-1020 Vienna, Austria*

(Received 24 May 1991)

The coherent overlap of the waves traversing the two legs of a perfect-crystal neutron interferometer is altered by a material with a neutron-nuclear optical potential. The fringe visibility is limited by the longitudinal coherence length. The loss of interference contrast caused by a slab of material of positive optical potential can be restored by placing another slab of material with a negative optical potential in the same leg of the interferometer. This paper describes the observation and detailed characterization of this quantum-mechanical phenomenon, which we call the phase-echo effect.

PACS number(s): 03.65.Bz, 42.50.−p

### I. INTRODUCTION

Quantum mechanics describes a moving neutron in terms of its wave function $\Psi(\mathbf{r},t)$. In an eigenstate

$$\Psi(\mathbf{r},t)=\psi(\mathbf{r})e^{-i\omega t}, \tag{1}$$

where the spatial part $\psi(\mathbf{r})$ satisfies the time-independent Schrödinger equation for a particle of mass $m$, momentum $\mathbf{p}$, and energy $E$:

$$\left[-\frac{\hbar^2}{2m}\nabla^2+V(\mathbf{r})\right]\psi(\mathbf{r})=E(\omega)\psi(\mathbf{r}) . \tag{2}$$

A monochromatic plane wave of amplitude $a(\mathbf{k})$,

$$\Psi(\mathbf{r},t)=a(\mathbf{k})e^{i(\mathbf{k}\cdot\mathbf{r}-\omega_k t)}, \tag{3}$$

where $\mathbf{k}=\mathbf{p}/\hbar$ and $\omega_k=E/\hbar=\hbar k^2/2m$, is a solution of this equation. But, it is of infinite spatial extent. The idea of a particle such as the neutron having infinite spatial extent is intuitively unappealing. To localize the probability amplitude of the neutron, one superposes a series of plane waves whose wave vectors differ slightly, so that they add constructively in some finite region of space and time, but sum to zero elsewhere. This creates a localized "wave packet," which more closely corresponds to our classical idea of a moving, finite particle. Mathematically, we build the wave packet by a Fourier sum of plane-wave components, having a (complex) spectrum $a(\mathbf{k})$:

$$\Psi(\mathbf{r},t)=\int a(\mathbf{k})e^{i(\mathbf{k}\cdot\mathbf{r}-\omega_k t)}d\mathbf{k} . \tag{4}$$

The phases of the component waves are correlated by $a(\mathbf{k})$, so that they add constructively in some localized region of space-time, and cancel out elsewhere.

Consider a neutron wave packet $\Psi_i$ incident on a perfect Si crystal neutron interferometer (NI), as shown in Fig. 1 [1,2]. The first crystal blade of the NI splits the amplitude of $\Psi_i$ into two parts $\Psi_1$ and $\Psi_2$, which separate and traverse paths I and II, respectively. Both beams pass through an aluminum slab, which we can rotate through small angles $\alpha$ about a vertical axis. This slab, called the "phase rotator," changes the phases of $\Psi_1$ and $\Psi_2$ by amounts $\beta_1(\alpha)$ and $\beta_2(\alpha)$, respectively. The beam $\Psi_2$ also passes through a plane-parallel slab of some material, perpendicular to the beam, with atom density $N$, neutron-nuclear scattering length $b$, and thickness $D$. This slab, which we call the "sample," induces a phase shift

$$\chi_S=k\Delta l=-\frac{2\pi NbD}{k}=-NbD\lambda \tag{5}$$

and a spatial delay

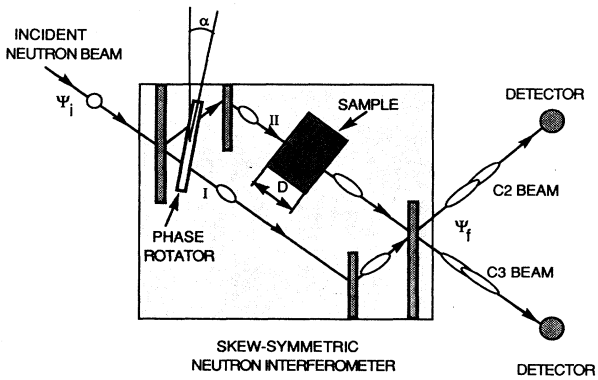


FIG. 1. Schematic of a neutron wave packet passing through a skew-symmetric neutron interferometer, with a phase rotator across both beams and a sample of some material in beam II.

 

$$\Delta l = -\tfrac{1}{2} D V_{\rm op}/E \tag{6}$$

in $\Psi_2$, where $E$ is the neutron's kinetic energy and $V_{\rm op}$ is the neutron-nuclear optical potential ($2\pi\hbar^2 Nb/m$). We assume for the moment that the sample does not attenuate the beam. The two waves recombine in the last perfect-crystal slab of the NI, and form two exit waves, which are linear combinations of $\Psi_1$ and $\Psi_2$. If the optical path lengths of beams I and II are nearly equal, the two packets overlap and coherently interfere, giving rise to interference effects.

The cumulative effect of passing through the NI is that each component of the wave packet has its amplitude reduced by a factor $\gamma$, and experiences a dispersive phase shift, such that

$$\Psi_1 = \int a(\mathbf{k}) \gamma_1 e^{i(\Phi_1+\beta_1)} e^{i\omega_k t} , \tag{7}$$

$$\Psi_2 = \int a(\mathbf{k}) \gamma_2 e^{i(\Phi_2+\beta_2+\chi_S)} e^{i\omega_k t} , \tag{8}$$

where $\Phi_1$ and $\Phi_2$ are the phase changes that occur in an empty NI, due to passage through the crystal blades and the regions between the blades. Under ideal conditions, $\Phi_1 = \Phi_2$ The phase angles $\Phi_{1,2}$, $\beta_{1,2}$, and $\chi_S$ depend on the wave vector $k$. The factors $\gamma_{1,2}$ and $\Phi_{1,2}$ depend on which exit beam, $C2$ or $C3$, we are considering. As a result, the wave functions $(\Psi_1)_{C2}$ and $(\Psi_2)_{C2}$ which enter the $C2$ exit beam differ from $(\Psi_1)_{C3}$ and $(\Psi_2)_{C3}$, which enter the $C3$ beam. The exit wave function $\Psi_f$ is the sum of $\Psi_1$ and $\Psi_2$; consequently, the two exit waves $[(\Psi_f)_{C2} = (\Psi_1)_{C2} + (\Psi_2)_{C2}$ and $(\Psi_f)_{C3} = (\Psi_1)_{C3} + (\Psi_2)_{C3}]$ differ in amplitude and phase. If one of the exit beams enters a detector large enough to fully encompass it, the time-averaged counting rate in the detector is

$$\begin{aligned} I &= \lim_{T\to\infty} \frac{1}{T} \int_0^T dt \int_{-\infty}^{+\infty} \Psi_f^*(\mathbf{k}) d\mathbf{k} \int_{-\infty}^{+\infty} \Psi_f(\mathbf{k}') d\mathbf{k}' \\ &= \lim_{T\to\infty} \frac{1}{T} \int_0^T dt \int_{-\infty}^{+\infty} d\mathbf{k} \int_{-\infty}^{+\infty} dk' a(\mathbf{k}) a^*(\mathbf{k}') [(\gamma_1)^2 + (\gamma_2)^2 \\ &\quad + \gamma_1\gamma_2 (e^{i[\phi_0+\phi_P(\alpha)+\chi_S]} + e^{-i[\phi_0+\phi_P(\alpha)+\chi_S]}) ] e^{-i(\mathbf{k}\cdot\mathbf{r}-\omega_k t)} e^{i(\mathbf{k}'\cdot\mathbf{r}-\omega_k' t)} . \end{aligned} \tag{9}$$

We define the initial phase difference to be

$$\phi_0 \equiv \Phi_2 - \Phi_1 , \tag{10a}$$

and the phase shift due to the phase rotator is

$$\phi_P(\alpha) = \beta_2(\alpha) - \beta_1(\alpha) = N_P b_P \lambda d \frac{\sin^2\theta_I \sin\alpha}{\cos^2\theta_I - \sin^2\alpha} , \tag{10b}$$

where $N_P$, $b_P$, and $d$ are, respectively, the atom density, nuclear scattering length, and thickness of the phase rotator; $\theta_I$ is the Bragg angle of the interferometer. The $\mathbf{k}$ and $\mathbf{k}'$ dependence of these phase angles has been suppressed, for notational simplicity. The integral over time $t$ yields a delta function $\delta(\omega_k - \omega_k')$, so that

$$\begin{aligned} I(D,\alpha) &= A \int_{-\infty}^{+\infty} |a(\mathbf{k})|^2 d\mathbf{k} \\ &\quad + B \int_{-\infty}^{+\infty} |a(\mathbf{k})|^2 \cos[\phi_0 + \phi_P(\alpha) + \chi_S(D)] d\mathbf{k} , \end{aligned} \tag{11}$$

where we have defined

$$A \equiv \gamma_1^2 + \gamma_2^2, \quad B \equiv 2\gamma_1\gamma_2 . \tag{12}$$

We explicitly note the dependence of the average counting rate on the thickness of the sample $D$ and the angle $\alpha$ of the phase rotator, since these are the parameters that are varied in our experiment. Since $\gamma_1$ and $\gamma_2$ differ for the $C2$ and $C3$ beams, the parameter $A$ has a different value in the two exit beams [3].

The first integral term in Eq. (11) is a constant. The second term, however, oscillates as we vary $\phi_P(\alpha)$. For example, if the spectral distribution $g(\mathbf{k}) = |a(\mathbf{k})|^2$ is a Gaussian, of standard deviation $\sigma_k$, then Eq. (11) yields an intensity

$$I(D,\alpha) = A + B \cos[\phi_0 + \phi_P(\alpha) + \chi_s(D)] e^{-(NbD\sigma_\lambda)^2/2} , \tag{13}$$

where $\sigma_\lambda = 2\pi\sigma_k/k^2$ is the width of the spectral distribution in terms of wavelength $\lambda$ [4].

As we vary $\phi_P(\alpha)$, we trace out a sinusoidal intensity pattern $I(D,\alpha)$, called an interferogram. The first term in Eq. (13) gives the mean value of the pattern, while the second term describes the interference oscillations. The contrast (fringe visibility) of the interferogram is defined to be the amplitude of the oscillation divided by the mean value of the pattern. As Eq. (13) shows, the contrast $C(D)$ diminishes as the sample thickness $D$ increases; its maximum value $C(0)$ occurs when $D = 0$, that is, when there is no sample in beam II. In principle, the maximum contrast $C_{C3}(0)$ in the $C3$ beam may vary from 0% to 100%, depending on how well the interferometer performs; experimentally, we find $C_{C3}(0) \approx 50\%$. It is the relative contrast $C_R(D) \equiv C(D)/C(0)$ that is of interest in these experiments. The relative contrast can be calculated from the magnitude of the complex mutual coherence function $\Gamma(D,\alpha)$ [5]:

$$C_R(D) = \frac{C(D)}{C(0)} = \frac{|\Gamma(D,\alpha)|}{|\Gamma(0,0)|} , \tag{14}$$

where

$$\Gamma(D,\alpha)\equiv\langle\Psi_1^*(0)\Psi_2(\Delta l)\rangle$$
$$=\frac{1}{\sqrt{2\pi}}\int_{-\infty}^{+\infty}|a(\mathbf{k})|^2 e^{i[\phi_0+\phi_P(\alpha)+\chi_S(D)]}d\mathbf{k}\ . \quad (15)$$

Or, if the displacement $\Delta l$ is in the longitudinal direction (parallel to $\mathbf{k}$), we can use the wavelength spectrum $g(\lambda)$ to calculate $\Gamma(D,\alpha)$:

$$\Gamma(D,\alpha)=\frac{1}{\sqrt{2\pi}}\int_{-\infty}^{+\infty}g(\lambda)e^{i[\phi_0+\phi_P(\alpha)+\chi_S(D)]}d\lambda\ . \quad (16)$$

For our experiment $\chi_S(D)\gg\phi_P(\alpha)$, so that the phase rotator has negligible effect on the contrast. Thus, for a Gaussian distribution $|a(\mathbf{k})|^2$, the relative contrast falls [according to Eq. (13)] as a function of the sample thickness $D$ alone, namely

$$C_R(D)=e^{-(NbD\sigma_\lambda)^2/2}\ . \quad (17)$$

Such relative contrast curves were first measured for neutron interferometry by Kaiser, Werner, and George [6].

Note that Eq. (11) for the intensity $I(D,\alpha)$ depends only on the magnitude of the spectrum $a(\mathbf{k})$. In taking the complex conjugate required by Eq. (9), all information about the phase correlation of the Fourier components comprising the wave packet is lost. There is then no way, by measuring $I(D,\alpha)$, to establish the phase correlation of the various Fourier components. The same results could be produced by an incoherent superposition of infinite, phase-uncorrelated, monochromatic plane waves, with an intensity distribution $g(\mathbf{k})=|a(\mathbf{k})|^2$ [7,8]. If we know the intensity spectrum $g(\mathbf{k})$ [or $g(\lambda)$], we can predict the outcome of our $C_R(D)$ measurement; there is no need to refer to wave packets or localized neutrons, except at the moment of detection. From our continuous beam measurements, we cannot say for certain that the neutron travels as a packet, but only that the beam has an intensity spectrum $g(\mathbf{k})$ consistent with a traveling-wave packet.

There are therefore two conceptual interpretations as to why the relative contrast decreases with increasing sample thickness; both are equally valid. First, we known that a wave packet spreads as it propagates, with the faster wavelength components tending toward the leading end of the packet and the slower components toward the trailing end. The sample delays the packet on path II with respect to the packet on path I, so that when they reach the recombination region, the packets are spatially displaced by a distance $\Delta l(D)$,

$$\Delta l(D)=-\frac{\lambda^2 Nb}{2\pi}D\ . \quad (18)$$

Faster components within one packet then overlap with slower components within the other. The result is that the interference amplitude partially "washes out" when summed over the packet, which reduced the contrast of the interferogram [9]. If the two packets are displaced by a distance greater than the longitudinal coherence length, then the contrast disappears.

If one views the neutron beam as consisting of an incoherent superposition of plane waves, then a second conceptual interpretation can be applied: Each plane wave $k$ component gives rise to its own intensity pattern $I(k,D,\alpha)$; the overall intensity $I(D,\alpha)$ is the integral of $I(k,D,\alpha)$ over the intensity distribution $g(\mathbf{k})$. On passing through the sample, each component experiences a different phase shift $\chi_S(k,D)$, as given by Eq. (5). The overall intensity is thus a sum of sinusoidal patterns of differing phase, which leads to a reduction in interference amplitude. The beam is said to become "dephased" as the sample thickness increases, and the interferogram contrast eventually approaches zero.

## II. ATTENTUATION AND NONIDEAL EFFECTS

In this experiment, we wish to measure changes in interferogram contrast due to the coherence properties of a neutron beam. However, there are other effects which also reduce the contrast. These must be understood and corrected for, if we wish to isolate the dephasing effects.

First, we have to take into account the beam attenuation due to the sample, which we ignored in the preceding section. If an attenuating sample is placed in beam II, the amplitude of the wave $\Psi_2$ is attenuated by a factor $\exp(-\zeta)$, such that

$$\Psi_2=e^{-\zeta}\int a(\mathbf{k})(\gamma_2 e^{i(\Phi_2+\beta_2+\chi_S)})e^{i\omega_{\mathbf{k}}t}\ , \quad (19)$$

where $\zeta$ is due to the absorption and scattering cross sections $\sigma_a$ and $\sigma_s$ of the material:

$$\zeta(D)=\tfrac{1}{2}(\sigma_a+\sigma_s)ND\ . \quad (20)$$

The factor of $\frac{1}{2}$ is present because we are interested in the attenuation of the wave amplitude. Where the wave $\Psi_2$ in Eq. (8) was attenuated by a factor $\gamma_2$, it is now attenuated by a factor $\gamma_2 e^{-\zeta}$. So if we replace each factor of $\gamma_2$ in Eq. (12) with $\gamma_2 e^{-\zeta}$, we find that the mean value and amplitude parameters $A$ and $B$ are no longer constants, but vary with sample thickness as

$$A(D)=\gamma_1^2+e^{-2\zeta(D)}\gamma_2^2,\quad B(D)=2\gamma_1\gamma_2 e^{-\zeta(D)}\ . \quad (21)$$

The contrast is proportional to $B/A$, so that even in the absence of dephasing effects, attenuation leads to a loss in contrast with increasing sample thickness,

$$\left[\frac{C(D)}{C(0)}\right]_{\text{att}}=\frac{e^{-\zeta}}{a_{\text{I}}+e^{-2\zeta}a_{\text{II}}}\ , \quad (22)$$

where we define the intensity fractions $a_{\text{I}}$ and $a_{\text{II}}$ to be

$$a_{\text{I}}\equiv\frac{\gamma_1^2}{\gamma_1^2+\gamma_2^2},\quad a_{\text{II}}\equiv\frac{\gamma_2^2}{\gamma_1^2+\gamma_2^2}\ , \quad (23)$$

and where $a_{\text{I}}+a_{\text{II}}=1$. Thus, if we measure a contrast $C_{\text{meas}}$ in our experiment, and wish to deduce the contrast $C$ that would occur without the sample's attenuation, we merely multiply $C_{\text{meas}}$ by an attenuation correction factor $f_{\text{att}}$:

$$C=C_{\text{meas}}f_{\text{att}}\ , \quad (24)$$

where

$$f_{\text{att}}=e^{\zeta}[a_{\text{I}}+e^{-2\zeta}a_{\text{II}}] . \tag{25}$$

This gives us a way to measure the contrast $C$, correcting for and thereby excluding the effects of attenuation. The intensity fractions $a_{\text{I}}$ and $a_{\text{II}}$ and attenuation parameters $\zeta$ were measured experimentally, as described in the Appendix. From this information, we calculated the attenuation correction factors $f_{\text{att}}$ for each sample used, and corrected our results according to Eq. (24). (See the Appendix for details and results of this correction process.)

It is important to recall that the factors $\gamma_1$ and $\gamma_2$ are different for the two exit beams $C2$ and $C3$. Consequently, the intensity fractions $a_{\text{I}}$ and $a_{\text{II}}$ and the attenuation correction factors $f_{\text{att}}$ differ for $C2$ and $C3$. The effect of attenuation on the contrast of the two beams is therefore different, and we must correct the $C2$ and $C3$ data separately.

In addition to attenuation, there are other nonideal effects which reduce the interferogram contrast. In Sec. I, we assumed that the interferometer and setup were "ideal." That meant that the Si interferometer crystal was free from imperfections and machined to a flawless geometry: each blade equally spaced, flat, parallel, and of the same thickness. (The scale of this required precision is about 0.25 $\mu$m.) It also implied that the setup completely isolated the interferometer from outside disturbances, such as vibrations, rotations, and strains. With an arrangement such as this, we would be able to achieve perfect fringe visibility, yielding a contrast in the $C3$ beam of 100%. But this is, of course, not the case. At best, our neutron interferometer operates at a contrast of $\sim$70%, and usually less. This is because of small imperfections in the geometry of the NI and in the quality of the setup.

First, consider what happens if the surfaces of the interferometer blades are not completely flat and parallel. Thickness variations on the order of micrometers can easily be produced during the machining and etching of the crystal. A neutron ray striking a crystal blade at a given spot may thus pass through more material than a neutron striking another spot. As a result, the initial phase $\phi_i$ of the neutrons varies spatially across the cross sectional area of the beam. (The subscript "0" on $\phi_0$ has been changed to "$i$" to emphasize that the initial phase is now spatially variable.)

A simple model shows how such spatial inhomogeneities in the thickness of the blades lead to a loss in contrast. Consider a neutron beam incident on a region "$S$" on the first blade of the interferometer. A neutron striking the blade at point $(x,y)$ splits and moves through the NI, also passing through the other blades before recombining and finally being detected. Suppose the interferogram for the neutrons entering at $(x,y)$ has an initial phase $\phi_i(x,y)$, such that the resulting intensity is

$$I(x,y,\phi)=A+B\cos[\phi_i(x,y)+\phi(\alpha,D)] , \tag{26}$$

where $\phi(\alpha,D)=\phi_P(\alpha)+\chi_S(D)$. The overall intensity is the integral of $I(x,y,\phi)$ over region $S$:

$$I(\phi)=\int_S\{A+B\cos[\phi_i(x,y)+\phi(\alpha,D)]\}dx\,dy . \tag{27}$$

For our purposes here, $\phi(\alpha,D)$ is a constant. Within the illuminated area $S$, there is a probability distribution $w_s(\phi_i)$ of $\phi_i$ values. For the sake of discussion, we suppose that $w_s(\phi_i)$ is a Gaussian of width $\sigma_s$, centered at $\phi_s$ ("$s$" for "spatial"):

$$w_s(\phi_i)=\frac{1}{\sqrt{2\pi}\sigma_s}e^{-(\phi_i-\phi_s)^2/2\sigma_s^2} . \tag{28}$$

We replace the integral over $x$ and $y$ in Eq. (27) with one over the initial phase $\phi_i$, weighted by $w_s(\phi_i)$:

$$\begin{aligned}I(\phi)&=\int_{-\infty}^{+\infty}w_s(\phi_i)\{A+B\cos[\phi_i(x,y)+\phi(\alpha,D)]\}d\phi_i\\&=A+B\cos[\phi_s+\phi(\alpha,D)]e^{-\sigma_s^2/2} .\end{aligned} \tag{29}$$

Theoretically, $A$ and $B$ should be equal in the $C3$ exit beam. If there were no imperfections ($\sigma_s=0$), then $I_{C3}(\phi)$ would yield 100% contrast. However, we see that spatial inhomogeneities cause the amplitude of $I(\phi)$ to be reduced by a factor $\exp(-\sigma_s^2/2)$. Consequently, the contrast $C_s$ also drops by the same factor:

$$C_s=C_0e^{-\sigma_s^2/2} . \tag{30}$$

For example, if there were thickness variations of order $\Delta t=25$ $\mu$m across the illuminated area $S$, then there would be a phase uncertainty $\sigma_s$ of

$$\sigma_s=\frac{Nb_c\lambda\Delta t}{\sqrt{8\ln 2}}\approx 0.52\text{ rad}\approx 30^\circ \tag{31}$$

for $\lambda=2.349$-Å neutrons. As a result, no matter how good our setup was, we would not be able to produce a contrast higher than about $C_s\approx 87\%$ in $C3$ (and $\sim$30% in $C2$) due to the uneven blade surfaces.

Other "nonideal" contrast effects are due to vibrations and rotations transmitted to the interferometer crystal through the setup from the surrounding environment. The back and forth rotation of the interferometer causes the diffracted neutrons to be Doppler shifted upon reflection, so that the initial phase $\phi_i$ also varies with time. This shift in phase, due to rotation, is called the Sagnac effect [10].

This "temporal fluctuation" can be modeled in the same way as the spatial variations. If we assume that the time-varying initial phase $\phi_i(t)$ is described by a Gaussian distribution $w_t(\Delta\phi)$, of width $\sigma_t$ ("$t$" for "temporal"), we find that this leads to a further reduction in the time-averaged contrast by a factor $\exp(-\sigma_t^2/2)$. Combining the effects of spatial inhomogeneities and temporal fluctuations, the overall contrast $C_{s,t}$ is found to be reduced by both effects:

$$C_{s,t}=e^{-\sigma_s^2/2}e^{-\sigma_t^2/2} . \tag{32}$$

There are other effects that also reduce the interferogram contrast, such as thermal gradients, imperfections in machining, and gravitational warping of the crystal. In light of this discussion, it is not surprising that we cannot attain 100% contrast with our interferometer. In

fact, given its sensitivity to small imperfections and disturbances, it is quite a feat (perhaps a miracle) that the device works at all. We must content ourselves with a maximum contrast $C_0$ of $\sim 50\%$, and work from there.

## III. THE PHASE-ECHO EFFECT

In Sec. I, we saw that a sample placed in one leg of the interferometer shifts the packet on that path with respect to the other path (or, equivalently, that it dephases the Fourier components that make up the beam). As the sample thickness increases, the coherence of the beams is reduced, leading to a loss in interferogram contrast. For a Gaussian spectrum $g(\lambda)$ of width $\sigma_\lambda$, we found that the contrast also falls off as a Gaussian [Eq. (17)].

Now consider what happens if we add a second sample to the same leg of the interferometer. The second sample may be of a different material, so that its parameters $(N_2,b_2,D_2)$ may differ from those of the first sample $(N_1,b_1,D_1)$. The outcome of such an arrangement is not difficult to derive because the effect of the two samples is additive. For example, if we have a Gaussian $g(\mathbf{k})$, the relative contrast $C_R(D_1,D_2)$ is found from Eq. (17) simply by replacing the factor $(NbD)$ by $(N_1b_1D_1+N_2b_2D_2)$, so that the relative contrast becomes

$$C_R(D_1,D_2)=e^{-(N_1b_1D_1+N_2b_2D_2)^2\sigma_\lambda^2/2} . \tag{33}$$

The form of this equation presents us with an interesting possibility. For most nuclei, $b$ is positive, but there are a few elements, such as titanium, manganese, and vanadium, whose scattering lengths are negative. Thus, in contrast to x-ray and optical interferometry, we have a unique opportunity in neutron interferometry to place materials of both positive and negative optical potentials in one leg of the interferometer. If we choose one sample with a positive scattering length $b_1>0$ and another with a negative scattering length $b_2<0$ and machine them to thicknesses $D_1$ and $D_2$ such that

$$N_1b_1D_1=-N_2b_2D_2 , \tag{34}$$

then Eq. (33) implies that the relative contrast due to this arrangement is

$$C_R(D_1,D_2)=e^{-0}=100\% . \tag{35}$$

This means that there should be no loss in contrast (or coherence) due to the samples. When each sample is placed individually in the neutron beam, the coherence is reduced, resulting in a lower interferogram contrast. If, however, both samples are simultaneously placed in the same leg of the interferometer, the coherence of the beam is apparently restored. The first sample shifts the packet by $\Delta l$ (i.e., dephases the beam); but the second sample shifts the packet back by $-\Delta l$; it "rephases" the beam. We call this the "phase-echo effect." It was first proposed as an NI experiment by Badurek, Rauch, and Zeilinger in 1979 [11]. In one instance, the effect was observed by Kaiser, George, and Werner, in conjunction with another experiment, but was not studied systematically [12].

If the samples are not ideally matched, the contrast only partially recovers, but if the condition in Eq. (34) is exactly met, the relative contrast should recover to 100%. There will still be a loss of contrast due to attenuation by the samples, but this can be corrected for, as discussed in Sec. II. It is important to note that the effect occurs in both the $C2$ and $C3$ exit beams because the relative contrast $C_R$ has the same form for each beam. We can thus use data obtained from both detectors.

The paragraphs above assume that the intensity spectrum $g(\mathbf{k})$ is a simple Gaussian. Since this was not the case experimentally, we need to extend our analysis to general spectra. This is easy to do, however. If we measure $g(\mathbf{k})$ [or $g(\lambda)$], we can place it in Eq. (16), and calculate (numerically, if necessary) the predicted behavior of $C_R(D)$ using Eq. (14).

## IV. SAMPLES AND SETUP

To observe the phase-echo effect, the first order of business was to construct a suitable set of phase shifting samples. We chose to use bismuth and titanium. Bismuth has a large, positive scattering length $b=8.533$ fm, an atom density $N=2.82\times10^{28}$ m$^{-3}$, and a relatively low absorption cross section ($\sigma_a=0.0388$ barn and $\sigma_s=9.156$ barn). Titanium was chosen because it is one of the few materials with a large, negative scattering length, $b=-3.438$ fm; it has an atom density $N=6.031\times10^{28}$ m$^{-3}$. It is, however, more highly absorbing than bismuth: $\sigma_a=6.1$ barn and $\sigma_s=4.06$ barn.

Initially, five slab-shaped samples of bismuth and titanium were machined, polished, and etched, and then epoxied onto aluminum mounting brackets. The bismuth samples were made so that their nominal thicknesses were multiples of 4 mm (4, 8, 12, 16, and 20 mm). The titanium samples were made in multiples of 5 mm (5, 10, 15, 20, and 25 mm). The exact thicknesses of the samples are given in Table I. The samples were made in matching sets, one Bi and one Ti piece per set, and the sets were labeled 1–5, in order of increasing thickness. Within each set, the corresponding Bi and Ti samples were made such that the ratio of their thicknesses would give rise to the optimum phase-echo effect. From Eq. (34), the optimal ratio should be

$$\frac{D_{\mathrm{Ti}}}{D_{\mathrm{Bi}}}=\frac{-N_{\mathrm{Bi}}b_{\mathrm{Bi}}}{N_{\mathrm{Ti}}b_{\mathrm{Ti}}}=1.16 . \tag{36}$$

Due to the difficulty in machining bismuth, the actual thickness ratios were closer to 1.24. This means that the phase-echo contrast should not recover to a full 100%; but it should recover to nearly that level (at least 97% for our samples).

In addition, we made a sixth pair of Bi and Ti samples, which were thinner than the other sets (2.1 and 2.8 mm, respectively). Since this pair of samples was about half as thick as set 1, it was dubbed set $\frac{1}{2}$. These thinner samples were used in combination with larger samples to give finer increments in thickness. For example, bismuth samples 1 and $\frac{1}{2}$ could be used simultaneously to place 6.10 mm of Bi in the beam; we called such a combination

"bismuth sample $1\frac{1}{2}$." The thin samples in set $\frac{1}{2}$ could also be combined with the other samples, to create "sample $2\frac{1}{2}$," "sample $3\frac{1}{2}$," and so on. This effectively doubled the number of data points that we could obtain.

The basic setup for the phase-echo experiment is indicated schematically in Fig. 2. A slit 4 mm wide and 6 mm high was mounted ~7 cm in front of the interferometer, to restrict the beam size. When no sample was in the beam, this produced an average counting rate of ~530 counts/min with ~57% contrast in the $C3$ detector and a rate of ~2000 counts/min with ~17% contrast in the $C2$ detector. The Bi and Ti samples were affixed by means of their mounting brackets to an aluminum bar, which held the samples at the right height and position to intercept the beam. The bar was attached to a translation table, so that the samples could be driven in and out of beam II by a computer-controlled stepping motor.

The neutrons were detected by $\frac{1}{2}$-in.-diam, cylindrical, 20-atm $^3$He detectors, which are essentially black to thermal neutrons. The $C2$ detector was mounted vertically ~20 cm past the NI. It was surrounded by a casing made of $B_4C$ powder suspended in epoxy, which absorbed

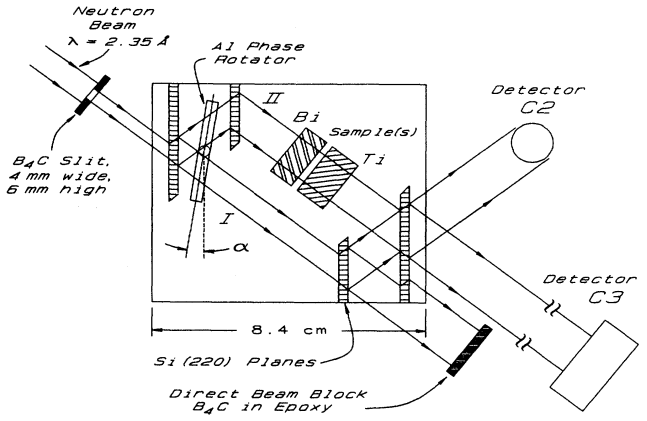


FIG. 2. Setup for the phase-echo experiment, sample-in condition, showing the width of the beam as it passes through the NI. The nominally monochromatic beam ($\Delta\lambda/\lambda=1.2\%$) is produced by Bragg reflection from a pyrolytic graphite monochromator ($2\theta_B=41°$). The Bragg angle of the (220) reflection in the silicon NI is $\theta_B=37.7°$.

TABLE I. Phase-echo relative-contrast results.

| Sample | $D$ (mm) | $\Delta l$ (Å) | $\Delta\phi$ (rad) | $(C_R)_{C2}$ (%) | $(C_R)_{C3}$ (%) | $\langle C_R \rangle$ (%) |
|---|---|---|---|---|---|---|
| | | | Bi | | | |
| $\frac{1}{2}$ | 2.09 | −44.2 | −118 | 87.3±1.6 | 83.5±1.7 | 86.5±0.8 |
| 1 | 4.01 | −84.7 | −227 | 51.8±1.4 | 59.0±1.6 | 52.6±0.8 |
| $1\frac{1}{2}$ | 6.10 | −128.9 | −345 | 24.4±1.1 | 21.1±1.3 | 24.4±0.6 |
| 2 | 7.99 | −168.8 | −452 | 4.3±0.9 | 7.8±1.1 | 4.2±0.5 |
| $2\frac{1}{2}$ | 10.08 | −213.0 | −571 | 13.0±0.8 | 16.4±1.1 | 13.5±0.4 |
| 3 | 12.26 | −259.1 | −694 | 14.1±0.8 | 14.8±1.1 | 12.7±0.4 |
| $3\frac{1}{2}$ | 14.35 | −303.2 | −812 | 3.3±0.8 | 8.3±1.2 | 4.0±0.4 |
| 4 | 16.15 | −341.2 | −914 | 1.5±0.8 | 0.3±1.3 | 1.3±0.4 |
| $4\frac{1}{2}$ | 18.24 | −385.4 | −1032 | 5.8±0.8 | 5.4±1.3 | 5.5±0.4 |
| 5 | 20.08 | −424.3 | −1135 | 3.6±0.8 | 3.4±1.3 | 3.8±0.4 |
| | | | Ti | | | |
| $\frac{1}{2}$ | 2.80 | 51.0 | 136 | 83.5±1.7 | 83.9±1.2 | 83.8±1.0 |
| 1 | 5.01 | 91.2 | 244 | 59.0±1.6 | 58.9±1.0 | 58.9±0.8 |
| $1\frac{1}{2}$ | 7.81 | 142.2 | 380 | 21.1±1.3 | 21.9±0.8 | 21.7±0.7 |
| 2 | 10.02 | 182.5 | 488 | 7.8±1.1 | 7.9±0.7 | 7.9±0.6 |
| $2\frac{1}{2}$ | 12.82 | 233.4 | 624 | 16.4±1.1 | 15.0±0.6 | 15.3±0.5 |
| 3 | 14.96 | 272.4 | 728 | 14.8±1.1 | 14.6±0.7 | 14.7±0.6 |
| $3\frac{1}{2}$ | 17.76 | 323.4 | 865 | 8.3±1.2 | 6.2±0.7 | 6.7±0.6 |
| 4 | 20.01 | 364.4 | 975 | 0.3±1.3 | 0.8±0.7 | 0.7±0.6 |
| $4\frac{1}{2}$ | 22.81 | 415.3 | 1111 | 5.4±1.3 | 5.6±0.7 | 5.6±0.6 |
| 5 | 24.98 | 454.9 | 1217 | 3.4±1.3 | 4.8±0.7 | 4.5±0.6 |
| | | | Bi+Ti | | | |
| $\frac{1}{2}$ | 4.89 | 6.8 | 18 | 99.7±2.4 | 101.4±1.5 | 100.9±1.3 |
| 1 | 9.02 | 6.5 | 17 | 91.2±2.2 | 89.9±1.4 | 90.2±1.2 |
| 2 | 18.01 | 13.7 | 36 | 91.9±2.1 | 92.7±1.3 | 92.5±1.1 |
| 3 | 27.22 | 13.3 | 35 | 99.4±2.4 | 95.3±1.4 | 96.4±1.2 |
| 4 | 36.16 | 23.2 | 61 | 115.0±2.8 | 106.9±1.6 | 108.9±1.4 |
| 5 | 45.06 | 30.6 | 82 | 91.1±2.6 | 89.9±1.5 | 90.2±1.3 |

any background neutrons. The beam was allowed to enter only through an opening, $\frac{1}{2}$ in. wide and 1 in. high, defined by a cadmium tube several inches long.

This phase-echo experiment was carried out in conjunction with a crystal-analyzed coherence experiment (to be described in a subsequent paper), and we wanted the setups for the two to be as similar as possible. For that reason, the $C3$ detector was mounted farther away, $\sim 80$ cm from the interferometer, and consisted of three $^3$He detectors, mounted horizontally in a neutron-shielding $B_4C$-epoxy cassette, which all fed into the same electronic counting chain.

The vast majority of neutrons entering the interferometer fall outside the Darwin acceptance width of the Si crystal, and are not diffracted. This so-called "direct beam" also has a divergence to it, and at the position of the $C3$ detector, it would partially overlap with the $C3$ beam, spilling into the detector and overwhelming the relatively weak $C3$ beam. To prevent this from happening, the direct beam was blocked with a 1-cm-thick slab of $B_4C$-epoxy directly after the NI.

## V. DATA COLLECTION AND ANALYSIS

As we have seen, even when there is no sample in the beam, a neutron interferometer operates at a contrast $C_0$ which is less than 100%. The goal of this experiment was to measure a drop in contrast from this starting value $C_0$ to a new value $C(D)$ when a sample was placed in the beam. The coherence loss due to the dephasing effect manifests itself in a *relative* drop in contrast from $C_0$ to $C(D)$. It was therefore important to measure the "sample-out" contrast $C_0$ as well as the "sample-in" contrast $C(D)$ for each data set.

The basic procedure consisted of taking simultaneous sample-out and sample-in interferograms. We first mounted a sample on the translation bar, but drove it to a position where it did not intercept the beam; we call this the sample-out position. With the phase rotator set to a certain position $\alpha_1$, data were collected until the monitor counter reached a fixed, preset number, usually 600-k monitor counts, taking approximately 3 min. In this period of time, the $C2$ and $C3$ detectors counted of order $\sim 1750$ and $\sim 6600$ neutrons, respectively. This is the sample-out data. We then drove the sample into the beam on leg II of the interferometer, and collected data again, usually for a longer time, $\sim 7$ min or so. This is the sample-in data. We then drove the sample back out of the beam, moved the phase shifter to a new position $\alpha_2$, and began the counting process again. After 30 or so data points, the result was a pair of interferograms, one with sample-out, and one with sample-in.

It was important to take these interferograms simultaneously because the absolute contrast $C_0$ drifted a small amount with time, due to environmental factors. Over the course of a day, the sample-out contrast $C_0$ might vary between 51% and 58%, although smaller drifts of $\sim \pm 1\%$ were usually the rule. However, the *relative* loss of contrast due to dephasing will *not* drift as long as the sample-in and sample-out curves had the same "starting" contrast $C_0$. To ensure that this was the case, we had to take the two data sets at the same time.

Collecting two such interferograms for a given sample constituted one data "run." The process was repeated for all Bi samples individually (including the paired $\frac{1}{2}$ samples), and then for all Ti samples as well. Finally, the matched sets of Bi and Ti samples were jointly mounted, one set at a time, and data runs were taken for these also. Each data run took between 7 and 20 h to complete. Longer counting times were used for thicker samples. This was partially to compensate for the reduction in beam intensity due to the attenuation of the sample. But the main reason for increasing the counting time was to improve the statistics for these runs. With thick samples, the contrast of the interferograms was severely reduced; only by increasing the counting time could we measure the small interferogram amplitudes with sufficient statistical accuracy. The background was checked periodically, but it varied little from day to day, so the measurements were averaged to give one, constant value, used throughout the experiment: $\mathcal{B}_{C2}=129$ counts/min, $\mathcal{B}_{C3}=29.7$ counts/min.

After completion, each interferogram was fit to a cosine function by a nonlinear least-squares-fit routine. The fit gives values for the amplitude $B$ and mean value $M$ of the interferogram; the mean value $M$ included the background rate $\mathcal{B}$ as well as the intensity $A$ due to the interfering neutrons: $M=A+\mathcal{B}$. The background rate $\mathcal{B}$ was measured separately by rotating the interferometer off the Bragg condition and counting. The measured value of $\mathcal{B}$ is used with the fit parameters $M$ and $B$ to calculate the contrast $C_{\text{meas}}$ of the interferogram:

$$C_{\text{meas}}=\frac{B}{M-\mathcal{B}} . \tag{37}$$

This was done separately for the data in both detector channels $C2$ and $C3$ for both the sample-out and sample-in conditions.

After fitting the sample-in interferograms, the contrast had to be corrected for attenuation due to the sample. We used the correction factors $f_{\text{att}}$ (given in Table III in the Appendix) to calculate the true, corrected contrast $C_{\text{in}}$,

$$C_{\text{in}}=(C_{\text{meas}})_{\text{in}} f_{\text{att}} . \tag{38}$$

Again, the correction had to be done separately for the $C2$ and $C3$ data since $f_{\text{att}}$ was different for the two exit beams. No such correction was required for the sample-out contrast $C_0$. The fit program also computed a statistical error for the mean value $M$ and amplitude $B$ of each fit. Likewise, the background counting rate $\mathcal{B}$ had a statistical uncertainty to it. Using standard statistical methods, we calculated error bars for our results.

The dephasing effect manifests itself in a drop in the relative contrast between the sample-out and sample-in data sets. If the sample-out contrast is $C_0 \pm \sigma_0$, and the sample-in contrast is $C_{\text{in}} \pm \sigma_{\text{in}}$, then the relative contrast $C_R \pm \sigma_R$ is given by

$$C_R=\frac{C_{\text{in}}}{C_0} , \tag{39}$$

where

$$\sigma_R = C_R \left[ \left[ \frac{\sigma_0}{C_0} \right]^2 + \left[ \frac{\sigma_{\text{in}}}{C_{\text{in}}} \right]^2 \right]^{1/2} . \quad (40)$$

Although the absolute contrasts $C_0$ and $C_{\text{in}}$ will differ for the $C2$ and $C3$ beams, the relative contrast $C_R$ should be the same for both, as discussed earlier. So, for each data run we can combine the $C2$ and $C3$ relative contrast results in the standard statistical way, weighting each according to its uncertainty. If the $C2$ relative contrast is $C_2 \pm \sigma_2$, and the $C3$ relative contrast is $C_3 \pm \sigma_3$, then the combined result $\langle C_R \rangle \pm \langle \sigma_R \rangle$ is given by

$$\langle C_R \rangle = \frac{(\sigma_3)^2 C_2 + (\sigma_2)^2 C_3}{(\sigma_3)^2 + (\sigma_2)^2} , \quad (41)$$

where

$$\langle \sigma_R \rangle = \left[ \frac{(\sigma_2 \sigma_3)}{(\sigma_2)^2 + (\sigma_3)^2} \right]^{1/2} . \quad (42)$$

The combined relative contrast $\langle C_R \rangle \pm \langle \sigma_R \rangle$ was the final, overall result of each data run.

## VI. RESULTS

Since the contrast results depend on the shape of $g(\mathbf{k})$, we first need to know the spectrum to be able to predict the outcome of the experiment. We actually chose to measure the intensity spectrum $g(\lambda)$ in terms of wavelength. A silicon (111) crystal with an effective mosaic width of $\sim 0.02°$ was placed in the exit $C3$ beam, in the antiparallel geometry. This crystal acts as an analyzer, reflecting out of the beam an extremely narrow band of wavelengths. A relationship between the angular position $\theta$ of the analyzer crystal and the wavelength $\lambda$ of the neutrons reflected out of the beam gives the spectrum $g(\lambda)$, obtained in a $\theta$-$2\theta$ scan with the analyzer crystal, namely

$$\lambda(\theta) = \lambda_0 \left[ 1 + (\theta - \theta_A) \frac{\cos(\theta_I)\cos(\theta_A)}{\sin(\theta_I - \theta_A)} \right]^{-1} , \quad (43)$$

where $\theta_I$ and $\theta_A$ are the Bragg angles of the interferometer and the analyzer crystal, respectively, and $\lambda_0$ is the mean wavelength. Since the spectrum deviates somewhat from a simple Gaussian form, we chose the next order of complexity, and modeled the spectrum as the sum of two independent Gaussians

$$g_{2G}(\lambda) = \frac{a_1}{\sqrt{2\pi}\sigma_1} e^{-(\lambda-\lambda_1)^2/2\sigma_1^2} + \frac{a_2}{\sqrt{2\pi}\sigma_2} e^{(\lambda-\lambda_2)^2/2\sigma_2^2} . \quad (44)$$

Figure 3 shows the wavelength intensity spectrum, with the background subtracted and the peak intensity spectrum, with the background subtracted and the peak intensity normalized to 1. The double-Gaussian fit is also shown, with the fit parameters

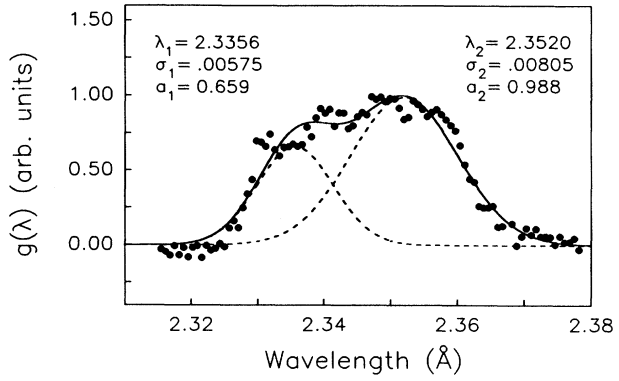


FIG. 3. Measured wavelength spectrum $g(\lambda)$ for the phase-echo experiment, and the double-Gaussian fit to it.

$$\lambda_1 = 2.3356 \text{ Å}, \quad \lambda_2 = 2.3530 \text{ Å} ;$$
$$\sigma_1 = 0.00575 \text{ Å}, \quad \sigma_2 = 0.00805 \text{ Å} ; \quad (45)$$
$$a_1 = 0.659, \quad a_2 = 0.988 .$$

The low signal to background ratio ($\sim 0.63$) limits the accuracy of these fit parameters. The actual spectrum may have more structure to it than is encompassed by a double-Gaussian distribution, but this approximation is sufficient for understanding the results of the experiment.

Let us now look at results of the phase-echo measurements. The data were collected in 26 data runs, and each was analyzed as described in Sec. V. Figure 4 shows a

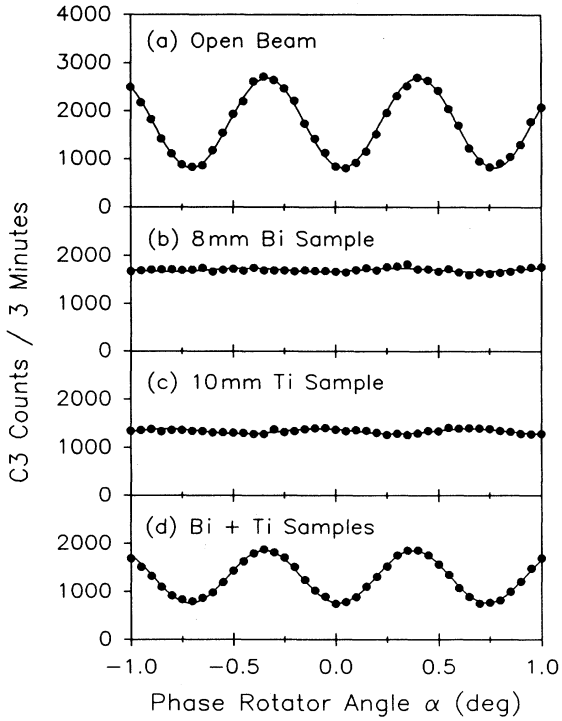


FIG. 4. A typical set of phase-echo interferograms, with (a) no sample, (b) with 8-mm Bi sample 2, (c) 10-mm Ti sample 2, and (d) both Bi 2 and Ti 2 in the beam.

typical set of data in the $C3$ detector channel, using samples from set 2 (8-mm Bi and 10-mm Ti). The interferograms originally had different counting times per data point, but the plots have been normalized to the same number of monitor counts per point, 600-k monitor $\approx 185$ sec. The solid curves show the least-squares fit to the data. The uppermost panel is for the sample-out condition, when both beams in the interferometer were unobstructed. Sample-out interferograms do not vary much from run to run, so only one representative example is shown. The second panel shows the interferogram when bismuth sample 2 (7.99 mm thick) was inserted into beam II; the third graph, when titanium sample 2 (10.02 mm thick) was used. In the bottom panel, Bi 2 and Ti 2 have been simultaneously inserted into the beam. The interferograms in Fig. 4 are thus the result of three different data runs.

The plots in Fig. 4 clearly show that the phase-echo effect does occur. When no sample was in the beam, the interferogram had relatively good contrast, $C_0 \approx 56\%$. When Bi or Ti alone was inserted, the contrast dropped considerably. Also, the counting rates of the sample-in curves were reduced due to the absorption of the samples; the loss is more pronounced for titanium, as one would expect. But, when Bi and Ti samples were jointly placed in the beam, the contrast recovers to a great extent. From the fits,

$$\begin{aligned} \langle C_R \rangle_{\mathrm{Bi}\,2} &= 4.17\% \pm 0.47\% \ , \\ \langle C_R \rangle_{\mathrm{Ti}\,2} &= 7.87\% \pm 0.58\% \ , \\ \langle C_R \rangle_{\mathrm{Bi+Ti}\,2} &= 92.5\% \pm 1.11\% \ . \end{aligned} \tag{46}$$

Each sample, when used independently, reduces the coherence of the beam, lowering the relative contrast to $\sim 6\%$. But by adding a second sample, the phase-echo effect restores the coherence, returning the relative contrast to nearly its full value, 92.5%.

The results shown above are for only one of the sample sets. A similar analysis was carried out for all of the remaining data runs. The resulting contrast data are summarized in Table I. Also given in the table are the phase shift $\Delta\phi$ and the longitudinal deviation $\Delta l$ caused by the sample(s). The columns labeled $(C_R)_{C2}$ and $(C_R)_{C3}$ give the relative contrasts for the $C2$ and $C3$ channels, corrected for attenuation; the final column $\langle C_R \rangle$ gives the weighted sum of the $C2$ and $C3$ data.

The data in Table I represent the overall results of the phase-echo experiment. Let us examine these results to see how well they agree with our predictions. First, let us look at the dephased data, when Bi or Ti were used alone. The relative contrast $C_R(D)$ in each case should fall off according to Eq. (14). Using our measured wavelength spectrum $g(\lambda)$, we can calculate what the contrast curve $C_R$ should look like. If we plot $C_R$ versus the phase shift $\Delta\phi = NbD\lambda$, then $C_R$ should look the same for both bismuth and titanium, and in fact for any phase-shifting material, given the same $g(\lambda)$. This has been done in Fig. 5, where $C_R$ is plotted for Bi samples alone and Ti samples alone versus $\Delta\phi(D)$. There is good agreement between the predicted and measured dephased contrast results. The measured Bi and Ti points trace out nearly identical curves, which are quite similar in shape to the predicted curve.

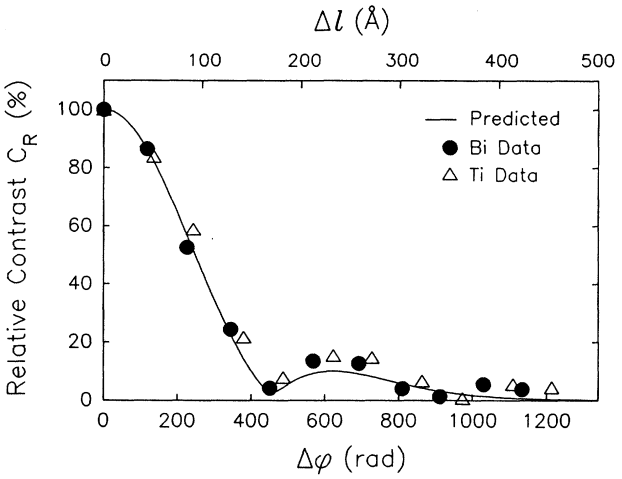


FIG. 5. Relative contrast results for both Bi and Ti samples used alone vs the total phase shift $\Delta\phi$. Also shown is the predicted contrast curve.

Of special interest in Fig. 5 is the fact that the contrast does not die out smoothly, but has a long "tail" to it. The existence of a tail on the contrast curve was original-

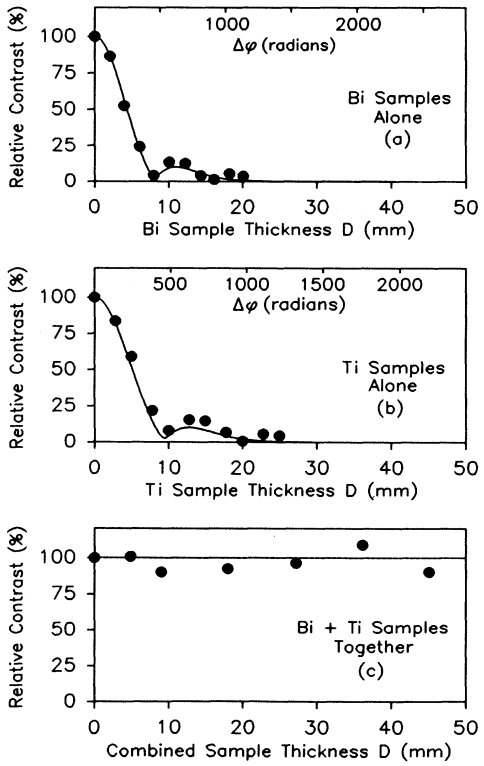


FIG. 6. Overall results of the phase-echo experiment, for (a) bismuth samples, (b) titanium samples, and (c) joint Bi+Ti samples. In all cases, the error bars are smaller than the plotted points.

ly perplexing to us, because we were not aware that the wavelength spectrum $g(\lambda)$ had a non-Gaussian shape. By measuring $g(\lambda)$, however, we were able to quite accurately explain the shape of the contrast tail.

So, the coherence loss due to dephasing occurs as predicted when bismuth or titanium samples are used individually. Let us now look at the results of the runs where Bi and Ti samples were used jointly, to see how the phase-echo effect alters the outcome. Figure 6 compares the dephased contrast curves, when Bi and Ti are used alone, to the phase-echo contrast curve, obtained when the matching Bi+Ti sets are used. The curves are plotted versus sample thickness $D$. The effect of the phase echo can be plainly seen. The top two graphs show that when Bi or Ti is used alone, the relative contrast falls off rather quickly and is practically zero when the sample thickness reaches $\sim$20 mm. But as is shown in the bottom graph, when both samples are used to create the phase-echo effect, the relative contrast remains very good, nearly 100%, all the way out to 45 mm, which is as much material as we could fit into our interferometer. This figure sums up the phase-echo effect in a concise way.

## VII. CONTRAST CURVES WITH NON-GAUSSIAN SPECTRA

The contrast curves measured in this experiment have a "two-humped" shape. As Eqs. (14) and (16) show, any deviation of the spectrum $g(\mathbf{k})$ from a simple Gaussian form will result in a contrast curve that is also non-Gaussian, although, as we shall see, this deviation may not always be experimentally visible.

This makes perfect sense mathematically, but let us try to gain some more physical insight into what is going on. We will use a simple model to investigate the effects of non-Gaussian spectra. For comparison, we would like the model to include the single-Gaussian spectrum as a special case. The simplest way to do this is to choose a model spectrum that consists of two equivalent Gaussian peaks $P_1$ and $P_2$, each with the same width $\sigma$ and amplitude, but centered at two different wavelengths $\lambda_1$ and $\lambda_2$. Placing such a spectrum in Eq. (15), we find that $C_R$ is given by

$$C_R(D)=|\cos(Nb_cD\Delta\lambda)|e^{-(Nb_cD\sigma)^2/2}, \tag{47}$$

where $\Delta\lambda=(\lambda_1-\lambda_2)/2$. Thus there is still a Gaussian decay in contrast, but it is modulated by a slowly oscillating cosine term. The first minimum of this cosine term is located at $D_{\min}=\pi/(Nb\Delta\lambda)$. At this point, the neutrons in peak $P_1$ are, on the average, 180° out of phase with those in peak $P_2$, so that their interferogram patterns cancel out, giving a contrast minimum. For the minimum to be visible, however, it must occur before the exponential decay has become too severe. If this is not the case, the contrast curve will still appear roughly Gaussian. If, on the other hand, $\Delta\lambda$ is large enough, then the contrast curve will oscillate within a Gaussian envelope. Although simple, this model adequately describes the physics behind the experimental contrast curves.

## VIII. CONCLUSIONS

From this experiment, we can say without a doubt that the phase-echo effect is a fact of nature as predicted by quantum mechanics. Figures 4 and 6 are the proof: 20 mm of bismuth destroys the coherence of the neutron beam; 25 mm of titanium also destroys the coherence; but put the two together, and the coherence recovers to nearly 100%.

This observation begs the following question. What do we mean when we say that the coherence is "lost" when a sample of optical potential $V_{\rm op}$ is placed in one leg of the interferometer? It can obviously be found again by placing yet another sample of optical potential $-V_{\rm op}$ in the same leg of the interferometer. Was it ever lost in the first place? The answer is that the coherence is only "apparently" lost. Each wavelength component produces two waves $\psi_{\rm I}$ and $\psi_{\rm II}$ traversing the interferometer, which are still perfectly coherent with each other. The coherence properties of each wavelength component remain intact, and each component is still related to all the other components in a definite way. In this sense, the neutron beam is still coherent, even after being dephased by the sample.

But we do not detect only one wavelength component. When we average our measurements over the spectral distribution $|a(\mathbf{k})|^2$, we find that the coherence properties of the various $\lambda$ components tend to cancel out when a thick sample is used. The fringe visibility becomes washed out in the overall beam, and is no longer macroscopically observable. In a very real sense, the beam then consists of a series of Fourier components, whose sum adds up to give zero contrast. Yet the phase coherence is still contained in the waves traversing the two legs of the interferometer, and can be reconstructed once again by the phase-echo effect.

## ACKNOWLEDGMENTS

This work was supported by the Physics Division of the NSF (Grant Nos. PHY-8813253 and PHY-9024608), the U.S.–Austria program at NSF (Grant No. INT-8712122), and Fonds zur Förderung der Wissenschaftlichen Forschung (Project No. S4201) in Austria.

## APPENDIX: MEASURING ATTENUATION CORRECTION PARAMETERS

To correct for attenuation, we need to know the intensity fractions $(a_{\rm I})_{C2,C3}$ and $(a_{\rm II})_{C2,C3}$ of the beams on path I and path II of the interferometer, for the $C2$ and $C3$ exit beams separately. We also have to know how the attenuation factor $\zeta(D)$ of the samples depends on the sample thickness $D$. Knowing this, the attenuation correction factors $(f_{\rm att})_{C2,C3}$ can be calculated for the two exit beams:

$$[f_{\rm att}(D)]_{C2,C3}=e^{\zeta(D)}[(a_{\rm I})_{C2,C3}+e^{-2\zeta(D)}(a_{\rm II})_{C2,C3}]\ . \tag{A1}$$

The intent of this appendix is to find a table of $f_{att}$ values for both the $C2$ and $C3$ exit beams, for the Bi and Ti samples used in our experiment. The setup is identical to that used in the experiment.

The first parameters to be measured were the intensity fractions $a_I$ and $a_{II}$. The measurement technique was rather simple. We first blocked beam II with a piece of cadmium, and measured the intensity $I_1$ due to neutrons path I alone, in both the $C2$ and $C3$ detectors. Then, leaving beam II blocked the interferometer was rotated off of its Bragg condition, so that no coherent beams were entering the detectors, and measured the background rate $\mathcal{B}_1$. We next returned the interferometer to the Bragg condition, moved the cadmium piece so that it blocked beam I instead, and measured the intensity $I_2$ due to the neutrons on path II alone, in both the $C2$ and $C3$ detectors. Finally, the interferometer was once more rotated off of the Bragg condition, and the background rate $\mathcal{B}_2$ was measured with beam I still blocked. From these data, we calculated $a_I$ and $a_{II}$.

Referring to the definitions of $a_I$ and $a_{II}$ in Eq. (23), the coherent beam intensities are related to our data by

$$(a_I)_{C2,C3}=\left[\frac{I_1-\mathcal{B}_1}{I_1-\mathcal{B}_1+I_2-\mathcal{B}_2}\right]_{C2,C3},$$
$$(a_{II})_{C2,C3}=\left[\frac{I_2-\mathcal{B}_2}{I_1-\mathcal{B}_1+I_2-\mathcal{B}_2}\right]_{C2,C3}. \tag{A2}$$

We measured the intensities $I_1$ and $I_2$ for $\sim 190$ sec, and then repeated the measurement ten times. The background rates $\mathcal{B}_1$ and $\mathcal{B}_2$ were measured for the same length of time, but only for six trials. From these data, the intensity fractions $a_I$ and $a_{II}$ were derived for both beams, as shown in Table II.

The next experimental step was to measure the attenuation factors $\zeta$ of the Ti and Bi samples. This was done by measuring the beam attenuation due to the samples. To mimic the actual experimental conditions as closely as possible, the transmission measurements were done in beam II of the interferometer. The other beam on leg I was blocked with a cadmium piece. This prevented the two beams from interfering with each other, so that the intensity rate in the two detectors would be constant, and not depend on any phase shift $\Delta\phi$. There was a possibility that neutrons could be small-angle scattered out of the beam, and yet still enter the $C3$ detector; for that reason, preference was given to the data collected in the $C2$ detector.

TABLE II. Measured intensity fractions $a_I$ and $a_{II}$ in both exit beams.

| Detector | $a_I$ | $a_{II}$ |
|---|---|---|
| $C2$ | 0.758±0.005 | 0.242±0.002 |
| $C3$ | 0.536±0.008 | 0.464±0.007 |

The technique used to measure the attenuation due to the samples is as follows. First, beam I was blocked with cadmium, but beam II was left open, with no sample in it. With this arrangement, we measured the sample-out intensity $I_{out}$ for about 55 min. Next, the sample was mounted in beam II, leaving beam I blocked, and the sample-in intensity $I_{in}$ was measured for the same length of time. Afterwards, the interferometer was rotated off its Bragg position, so that no beam diffracted onto path II. The neutron background $\mathcal{B}$ was measured for the same amount of time. Since there was no beam on path II, the background was the same whether there was a sample in place or not.

From these data, the transmission $T$ of the beam through the sample was calculated:

$$T=\frac{I_{in}-\mathcal{B}}{I_{out}-\mathcal{B}}. \tag{A3}$$

And from the transmission $T$ we calculated the absorption factor $\zeta$ of the sample:

$$\zeta=-\tfrac{1}{2}\ln T. \tag{A4}$$

TABLE III. Contrast attenuation correction factors $f_{att}$ for both $C2$ and $C3$ beams.

| Sample | $D$ (mm) | $(f_{att})_{C2}$ | $(f_{att})_{C3}$ |
|---|---|---|---|
| | Bi | | |
| $\frac{1}{2}$ | 2.09 | 1.010 | 1.002 |
| 1 | 4.01 | 1.020 | 1.003 |
| $1\frac{1}{2}$ | 6.10 | 1.031 | 1.006 |
| 2 | 7.99 | 1.042 | 1.008 |
| $2\frac{1}{2}$ | 10.08 | 1.054 | 1.011 |
| 3 | 12.26 | 1.066 | 1.015 |
| $3\frac{1}{2}$ | 14.35 | 1.079 | 1.019 |
| 4 | 16.15 | 1.090 | 1.023 |
| $4\frac{1}{2}$ | 18.24 | 1.104 | 1.027 |
| 5 | 20.08 | 1.116 | 1.032 |
| | Ti | | |
| $\frac{1}{2}$ | 2.80 | 1.057 | 1.012 |
| 1 | 5.01 | 1.109 | 1.029 |
| $1\frac{1}{2}$ | 7.81 | 1.185 | 1.059 |
| 2 | 10.02 | 1.253 | 1.091 |
| $2\frac{1}{2}$ | 12.82 | 1.351 | 1.141 |
| 3 | 14.96 | 1.435 | 1.186 |
| $3\frac{1}{2}$ | 17.76 | 1.557 | 1.257 |
| 4 | 20.01 | 1.667 | 1.322 |
| $4\frac{1}{2}$ | 22.81 | 1.818 | 1.416 |
| 5 | 24.98 | 1.948 | 1.498 |
| | Bi+Ti | | |
| $\frac{1}{2}$ | 4.89 | 1.069 | 1.016 |
| 1 | 9.02 | 1.136 | 1.039 |
| 2 | 18.01 | 1.326 | 1.127 |
| 3 | 27.22 | 1.578 | 1.269 |
| 4 | 36.16 | 1.905 | 1.470 |
| 5 | 45.06 | 2.316 | 1.737 |

Once again, there were actually two separate measurements of $\zeta$ for each data run, one in the $C2$ beam, and the other in the $C3$ beam. Such a transmission measurement was carried out for all six Ti samples. The results were plotted as a graph of $\zeta$ versus sample thickness $D$. According to Eq. (20), $\zeta$ should be a linear function of $D$. We fit a straight line to the plot, including the point $(D=0,\zeta=0)$, and used the slope of this line to calculate the experimental values of the absorption factor $\zeta$ for each sample. For the Ti samples, the result is

$$\zeta_{\mathrm{Ti}}(D_{\mathrm{Ti}})=(3.57\times10^{-2}\ \mathrm{mm}^{-1})D_{\mathrm{Ti}}\ . \tag{A5}$$

The process was then repeated for the Bi samples. A linear fit to the data points yields the result

$$\zeta_{\mathrm{Bi}}(D_{\mathrm{Bi}})=(9.41\times10^{-3}\ \mathrm{mm}^{-1})D_{\mathrm{Bi}}\ , \tag{A6}$$

With the experimentally measured values of $a_{\mathrm{I}}$, $a_{\mathrm{II}}$, and $\zeta$, the contrast attenuation correction factors $f_{\mathrm{att}}$ were calculated. The results are summarized in Table III.

*Present address: Physics Department, Bethany College, Bethany, WV 26032.

[1] H. Rauch, W. Treimer, and U. Bonse, Phys. Lett. A **47**, 3697 (1974); D. Petrascheck and R. Folk, Phys. Status Solidi A **36**, 147 (1976).
[2] V. F. Sears, *Neutron Optics* (Oxford University Press, Oxford, 1989), p. 245–252.
[3] H. Rauch and M. Suda, Phys. Status Solidi A **25**, 495 (1974).
[4] D. Petrascheck, Phys. Rev. B **35**, 6549 (1987).
[5] W. A. Hamilton, A. G. Klein, and G. I. Opat, Phys. Rev. A **28**, 3149 (1983).
[6] H. Kaiser, S. A. Werner, and E. A. George, Phys. Rev. Lett. **50**, 563 (1983).
[7] G. Comsa, Phys. Rev. Lett. **51**, 1105 (1983).
[8] H. Bernstein and F. Low, Phys. Rev. Lett. **59**, 951 (1987).
[9] A. G. Klein, G. I. Opat, and W. A. Hamilton, Phys. Rev. Lett. **50**, 563 (1983).
[10] S. A. Werner, J.-L. Staudenmann, and R. Colella, Phys. Rev. Lett. **42**, 1103 (1979).
[11] G. Badurek, H. Rauch, and A. Zeilinger, in *Proceedings of a Workshop on Neutron Spin Echo, Grenoble, 1979,* edited by F. Mezei, Lecture Notes in Physics Vol. **128** (Springer-Verlag, Heidelberg, 1980), p. 136.
[12] H. Kaiser, E. A. George, and S. A. Werner, Phys. Rev. A **29**, 2276 (1984).